PAPER

Understanding the growth and photoelectrochemical properties of mesocrystals and single crystals: a case of anatase TiO₂†

Zhensheng Hong,*[a] Hong Dai,[b] Zhigao Huang[a] and Mingdeng Wei*[c]

Anatase TiO₂ mesocrystals and single crystals with dominant {101} facets were successfully synthesized without any additives using titanate nanowires as precursors under solvothermal and hydrothermal conditions, respectively. It is proposed that the oriented self-assembly process for the formation of TiO₂ mesocrystals was controlled by the same thermodynamic principle as that of single crystals in this simple reaction system. Furthermore, the TiO₂ mesocrystals were applied in photoelectrochemical (PEC) water splitting and demonstrated much enhanced photocurrent, almost 191% and 274% compared with that of TiO₂ single crystals and commercial P25, respectively. Electrochemical impedance measurements under illumination revealed that the photocurrent increase was largely ascribed to the effective charge separation of electron–hole pairs and fast interfacial charge transfer. This could be attributed to the intrinsic characteristics of the mesostructured TiO₂ composed of highly oriented nanocrystal subunits offering few grain boundaries, nanoporous nature and a short transport distance.

Introduction

Recently, the conversion of solar energy to hydrogen *via* a photoelectrochemical (PEC) route has received increasing research interests.[1–3] Various active semiconductor nanomaterials, such as Si,[4] TiO₂,[5–8] Fe₂O₃[9,10] and ZnO,[11] have been adopted as photoanodes for this energy transformation. Among them, TiO₂ is one of the most promising candidates for photoelectrochemical conversion because it is highly resistant to photocorrosion, widely available, cheap and nontoxic.[7] Generally, TiO₂ nanoparticles were widely used as photoanode material for water splitting owing to the large surface area and short hole diffusion lengths.[5,7,8] However, the PEC properties of TiO₂ nanoparticles suffer from high charge recombination loss due to the electron trapping/scattering at grain boundaries (0.01 cm² V⁻¹ S⁻¹ for P25).[12,13] Nanostructured TiO₂ with well-developed morphology has been proved to demonstrate enhanced PEC performance due to its fast charge transport and efficient contact between the electrode and the electrolyte.[14–19] These include nanostructures composed of one-dimensional nanotubes/nanowires,[14–16] three-dimensional hierarchical architectures[17,18] and mesoporous structure.[19] From these studies, it is proved that high surface area, good light absorption, rapid charge transfer and effective charge separation of electron–hole pairs facilitate the efficient PEC conversion. Most recent research revealed that the fast charge transport played a key role in the PEC performance.[20] However, a perfect nanostructure which simultaneously addresses all these features for efficient PEC conversion has yet to be achieved.

Mesocrystals, a new class of ordered nanoparticle superstructures, were first found in biominerals and proposed by Cölfen and Antonietti in 2005.[21] Such mesoscopically structured crystals are constructed from crystallographically oriented nanocrystals (1–100 nm), which are conceptually different from nanocrystal superlattices.[22,23] Mesocrystals are porous quasi-single crystals, providing the advantages inherited from single crystals and the large surface area, and thus making them more promising for applications in catalysis, sensing and energy storage and conversion compared with single-crystalline or polycrystalline materials.[21,24,25] It is noteworthy that mesocrystals showed enhanced lithium-ion storage properties and excellent photocatalytic degradation of organic contaminants due to their high crystallinity, high porosity and oriented subunit alignment.[26–30] However, the properties of mesocrystals for PEC cells were rarely reported. So far, many kinds of mesocrystals such as minerals,[31,32] organic molecules[33] and metal oxides[24,25] have been reported. Generally, it is demonstrated that the formation of mesocrystals is from a so-called "non-classical crystallization", which involves the mesoscopic transformation

[a] *College of Physics and Energy, Fujian Normal University, Fuzhou, Fujian 350108, China. E-mail: winter0514@163.com*

[b] *College of Chemistry and Chemical Engineering, Fujian Normal University, Fuzhou, Fujian 350108, China*

[c] *Institute of Advanced Energy Materials, Fuzhou University, Fuzhou, Fujian 350002, China. E-mail: wei-mingdeng@fzu.edu.cn*

This journal is © the Owner Societies 2014

Phys. Chem. Chem. Phys., 2014, **16**, 7441–7447 | 7441

of self-assembled and metastable precursor particles into a single nanoparticulate superstructure.[34] However, the synthesis routes are materials dependent and the formation mechanism of mesocrystals is still a topic of research. It is very difficult to predict the morphology of mesocrystals using the thermodynamic concepts under nonequilibrium conditions because lots of organic additives were usually introduced into the mesoscale assembly process.

Herein, anatase TiO_2 mesocrystals and single crystals with dominant {101} facets, the most thermodynamic stable facet for anatase, were successfully synthesized using titanate nanowires as precursors under solvothermal (acetic acid) and hydrothermal conditions respectively. The mesocrystals were formed through the oriented self-assembly process of anatase nanocrystal subunits, and the single crystals were formed through the dissolution and recrystallization of TiO_2–B nanorods. Furthermore, the TiO_2 mesocrystals were applied in PEC conversion and demonstrated much enhanced photocurrent, almost 191% and 274% compared with that of TiO_2 single crystals and commercial P25, respectively.

Experimental

The anatase TiO_2 mesocrystals and single crystals were synthesized under solvothermal (HAc) and hydrothermal conditions, respectively, using titanate nanowires as precursors. Synthesis of titanate nanowires is similar to our previous work.[35] Typically, 1 g of TiO_2 (anatase) was dispersed in a 50 mL of 15 M aqueous KOH solution. After stirring for 10 min, the resulting suspension was transferred into a 75 mL teflon-lined stainless steel autoclave. The autoclave was kept at 170 °C for 72 h and then cooled to room temperature. The resulting precipitate was washed by diluted HAc solution until pH = 3.5 was reached. The final product was then collected by centrifugation and dried at 60 °C for 12 h in air. Synthesis of TiO_2 mesocrystals started with dispersing 200 mg of precursor titanate nanowires in 35 mL HAc solution (over 99%, weight), and then transferred into a 75 mL teflon-lined stainless steel autoclave, which was heated at 200 °C for 48 h. The final product was obtained by centrifugation and washed thoroughly with distilled water and ethanol, dried at 60 °C overnight, and calcined at 400 °C for 30 min to remove the residual organics. Synthesis of TiO_2 single crystals is similar to this process except heating under hydrothermal conditions for 72 h.

Scanning electron microscopy (SEM, S4800 instrument) and transmission electron microscopy (TEM, FEI F20 S-TWIN instrument) were applied for the structural characterization of the products. X-ray diffraction (XRD) patterns were recorded on a PANalytical X'Pert spectrometer using the Co Kα radiation (λ = 1.78897 Å), and the data were changed to Cu Kα data. The UV-visible measurements were performed on Perkin-Elmer Lambda 950. Infrared spectra of the samples were measured using a Fourier transform infrared spectrometer (FT-IR spectrometer spectrum 2000).

Photoelectrochemical (PEC) measurements were carried out in a quartz cell filled with a 0.5 M Na_2SO_4 electrolyte (pH = 6.9) with a conventional three-electrode process, which were performed on a CHI 660E electrochemical workstation. An Ag/AgCl electrode (sat. KCl) was used as a reference electrode, a platinum wire and a modified glassy carbon electrode (GCE, 3 mm in diameter) deposited with samples were used as an auxiliary electrode and a working electrode, respectively. For the preparation of electrode films, 3 mg mL^{-1} P25, TiO_2 single crystals and mesocrystal sample solutions (ethanol) were prepared. The sample solution (equal volume was adopted for three different samples) was deposited on the freshly prepared GCE surface, and placed it under an infrared lamp until the solvent was evaporated, then the electrode film (ca. 450 nm in thickness) was formed after it was cooled to room temperature. Intensity of the arriving ultraviolet (UV) light (λ = 390 nm) to the working electrode was around 86 mW cm^{-2}. Linear sweep voltammetry was carried out at a scan rate of 100 mV s^{-1}. Electrochemical impedance spectroscopy (EIS) measurements were performed from 0.1 Hz to 10 kHz.

Results and discussion

Fig. 1 shows the XRD patterns of the samples prepared under solvothermal and hydrothermal conditions. All the diffraction peaks can be well indexed to pure anatase TiO_2 (JCPDS 73-1764). The average crystallite size of TiO_2 mesocrystals was ca. 13 nm and 42 nm for single crystals, calculated by using the Scherer equation based on the (101) diffraction peak. This result suggests that TiO_2 mesocrystals have a smaller crystalline size than single crystals. The morphology of the TiO_2 mesocrystals was revealed by SEM and TEM images, as presented in Fig. 2. The rough surface of the nanoparticles could be clearly observed from Fig 2a. The TEM image (Fig 2b) further reveals that the bipyramidal-shaped nanoparticles with predominantly 40–60 nm in length are composed of nanocrystal subunits. It may be noted that a small number of twinned particles coexist with the individual particles. Fig. 2c exhibits a typical TEM image of a single nanoparticle, this confirms that the TiO_2 nanoparticle was constructed from tiny nanocrystal subunits. The SAED pattern in Fig 2c (inset) taken from the whole nanoparticle exhibits a "single-crystal-like" diffraction, suggesting that the tiny nanoparticle subunits were highly oriented, leading to the formation of bipyramidal nanoparticles elongated along the
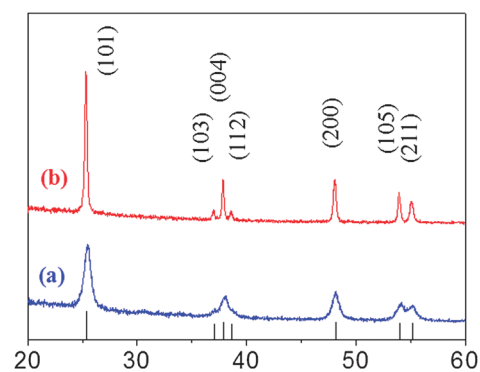

Fig. 1 XRD patterns of anatase TiO_2 mesocrystals (a) and single crystals (b) synthesized under solvothermal and hydrothermal conditions.

7442 | Phys. Chem. Chem. Phys., 2014, **16**, 7441–7447
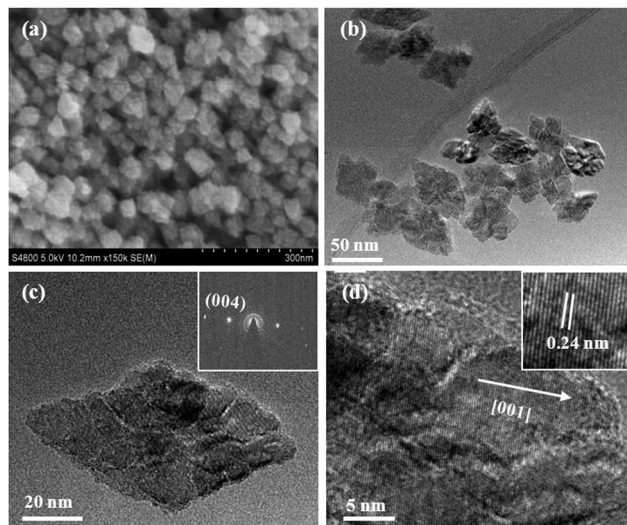
This journal is © the Owner Societies 2014

Fig. 2 SEM (a), TEM (b and c) and HRTEM (d) images of anatase TiO$_2$ mesocrystals synthesized under solvothermal conditions. The insets (c) and (d) are a SAED pattern and an enlarged HRTEM image.

[001] direction. The carefully obtained HRTEM image shown in Fig. 2d further confirms that the primary nanocrystals with 10–13 nm in size are highly crystalline, the clear lattice fringes of 0.24 nm well correspond to (004) spacing of the anatase structure. Furthermore, the internal porosity of the mesocrystals is also revealed by the HRTEM image. The nitrogen adsorption–desorption measurement (Fig. S1, ESI†) demonstrated that the Brunauer–Emmett–Teller (BET) surface area and the pore volume of TiO$_2$ mesocrystals were determined to be 88 m^2 g^{-1} and 0.36 m^3 g^{-1}, respectively. It is interesting that the size of a mesopore was about 18 nm, which could be attributed to the accumulation of the mesostructured particles.

The morphology of anatase TiO$_2$ single crystals was also characterized by SEM and TEM, as shown in Fig. 3. From the low

(Fig. 3a) and high magnification (Fig. 3b) SEM images, a large scale formation of uniform nanoparticles can be clearly observed. The TEM image (Fig. 3c) further confirms that the sample of anatase TiO$_2$ synthesized under hydrothermal conditions also has a bipyramidal shape with 30–60 nm in length. Fig. 3d presents a TEM image and the corresponding FFT pattern (inset) of a single nanoparticle, it is clearly shown that the anatase TiO$_2$ single crystals are highly crystalline with dominant {101} facets, which is a typical structure for anatase based on the Wulff constructions.

To elucidate the origin of the TiO$_2$ mesocrystals, a series of samples obtained from different reaction times were carefully characterized by XRD, SEM, TEM and FTIR. The XRD patterns (Fig. S2a, ESI†) reveal that the titanate nanowires were gradually transformed into anatase TiO$_2$. Fig. 4a–c show the SEM and TEM images of the samples obtained after a reaction time of 12 h, it can be observed that the titanate nanowire precursors were gradually decomposed and many tiny anatase nanocrystals (5–7 nm) were formed. When the reaction time increased to 24 h, the primary TiO$_2$ nanocrystals aggregated to form larger nano-particles, as shown in Fig. 4d and e. Fig. 4f presents a TEM image of a single loosened aggregate, which confirms that the aggregate was constructed by tiny nanocrystals ($\sim$10 nm). The FFT pattern depicted in Fig. 4f (inset) exhibits "single-crystal-like" diffraction spots, indicating that the tiny nanocrystal subunits were highly oriented in the same direction. Moreover, the nanocrystal subunits were partly recrystallized during the oriented self-assembly process. The emergence at 1560 and 1440 cm^{-1} in the FTIR spectra (Fig. S3, ESI†) could be indexed to the
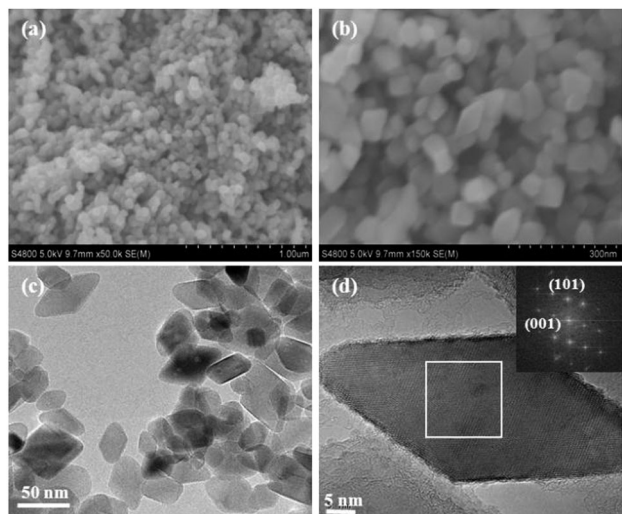

Fig. 3 SEM (a and b), TEM (c) and HRTEM (d) images of anatase TiO$_2$ single crystals synthesized under hydrothermal conditions. The inset in (d) is and a FFT pattern.
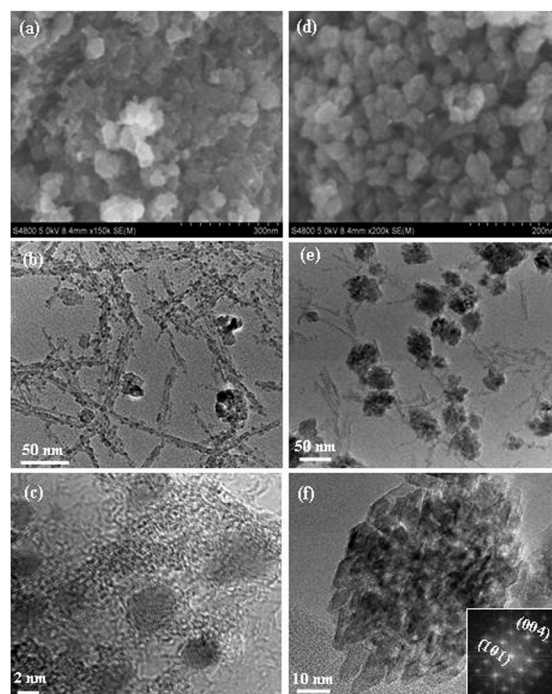

Fig. 4 SEM images (a and d) and TEM images (b, c, e, f) of the samples obtained from different reaction times under solvothermal conditions: (a–c) 12 h, (d–f) 24 h. The inset in (f) is the corresponding FFT pattern.

This journal is © the Owner Societies 2014

Phys. Chem. Chem. Phys., 2014, 16, 7441–7447 | 7443

asymmetric and symmetric stretching vibrations of the carboxylic group, suggesting the coordination of acetate to titanium.[36,37] TGA curves (Fig. S4, ESI†) further reveal that an amount of acetate or acetic acid (5.1%) was entrapped in TiO_2 mesocrystals.

The formation process of the TiO_2 single crystals was also carefully investigated by XRD, SEM and TEM. Interestingly, the XRD results (Fig. S2b, ESI†) reveal that the titanate precursor firstly transformed into TiO_2–B (JCPDS 74-1940), and then gradually transformed into anatase TiO_2 after 72 h. Fig. 5a–d show the SEM images of the samples obtained after the reaction time from 6 h to 48 h, it could be observed that the precursor titanate nanowires were firstly changed to nanorods (Fig. 5a), then more and more nanoparticles were formed with the increasing reaction times (Fig. 5b–d). Fig. 5e exhibits the TEM image of the sample obtained after the reaction time of 24 h, the clear lattice fringes (0.62 nm) of a nanorod shown in the inset can be well assigned to the (001) facings of TiO_2–B. A HRTEM image of a truncated-bipyramidal anatase nanocrystal and the tangent nanorods was shown in Fig. 5f, which reveals that the TiO_2–B nanorods were gradually dissolved accompanying *in situ* transformation into tiny anatase nanocrystals. In other words, the anatase single crystals were formed from the dissolution and recrystallization of TiO_2–B nanorods.

Generally, the mesocrystals were formed through nanoparticle oriented assembly, which is different from the classical crystallization way and was named as "non-classical crystallization".[24,34] It is widely reported that many organic or polymer additives

were usually added to assist the synthesis of mesocrystals.[21,24] The role of organic additives was to hinder the further growth of primary nanocrystals and/or could be considered as structure-directing agents for the self-assembled aggregation of nanoparticles to mesocrystals. Thus, it is very difficult to predict the morphology of mesocrystals using the thermodynamic concepts under nonequilibrium conditions. Although acetic acid has been used as the sole solvent for the nonhydrolytic synthesis of anatase mesocrystals without additives, various organisms were produced when the precursor of tetrabutyl titanate reacted with solvent.[26] In our current reaction system, both anatase TiO_2 mesocrystals and single crystals with similar size were successfully synthesized without any additives using titanate nanowires as precursors. Accordingly, a tentative mechanism for the formation of TiO_2 mesocrystals and single crystals was proposed as depicted in Fig. 6. Firstly, the precursors of titanate nanowires were gradually dissolved accompanying *in situ* transformation into tiny anatase nanocrystals stabilized by HAC under solvothermal conditions. The anatase mesocrystals were formed through the oriented self-assembly process of anatase nanocrystal subunits elongated along the [001] direction. However, the titanate nanowires were first transformed into TiO_2–B under hydrothermal conditions. The anatase single crystals were formed through the dissolution and recrystallization of TiO_2–B nanorods. Nevertheless, anatase TiO_2 mesocrystals and single crystals with dominant {101} facets and similar size were obtained at last. It is well documented that (101) is the most thermodynamically stable facet for anatase TiO_2.[38] Hence, the TiO_2 mesocrystals have common equilibrium shape with that of single crystals, suggesting that the growth of anatase mesocrystals was controlled by the same thermodynamic principle with single crystals in this simple reaction system and the mesocrystal is an intermediate of the single crystal. This result may provide a way to fabricate and predict the morphology of mesocrystals using the conventional thermodynamic principle.

Recently, there has been a great deal of interest in using nanostructured TiO_2 as photoanode material for the conversion of solar energy to hydrogen.[14–19] The anatase TiO_2 mesocrystals synthesized in this study offer much larger surface area, a shorter
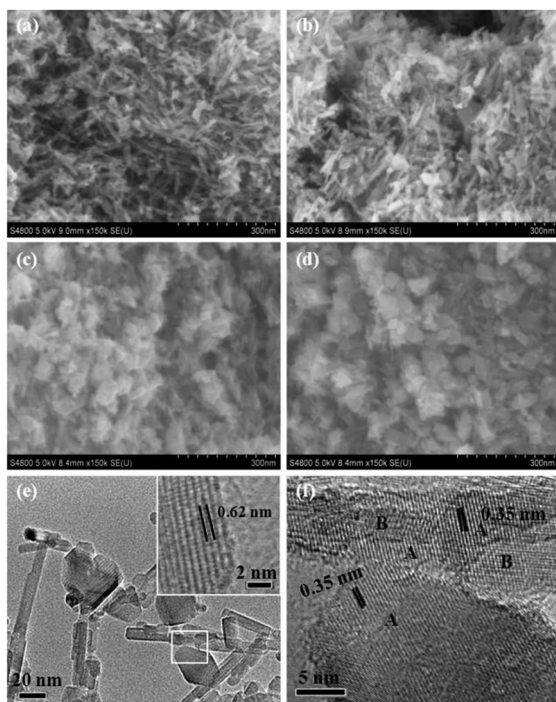

Fig. 5 SEM images (a–d), TEM (e) and HRTEM (f) images of the samples obtained from different reaction times under hydrothermal conditions: (a) 6 h, (b) 12 h, (c, e, f) 24 h, (d) 48 h. The inset in (e) shows a HRTEM image of a nanorod. The HRTEM image (f) was selected from the rectangular area in (e). A and B in (f) represent anatase TiO_2 and TiO_2–B, respectively.
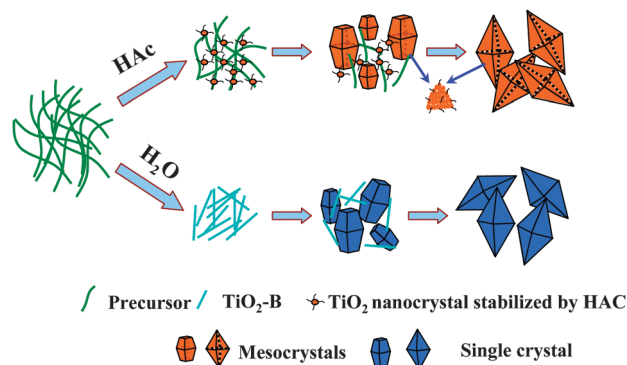

Fig. 6 Schematic of a tentative mechanism for the formation of TiO_2 mesocrystals.

7444 | *Phys. Chem. Chem. Phys.*, 2014, **16**, 7441–7447

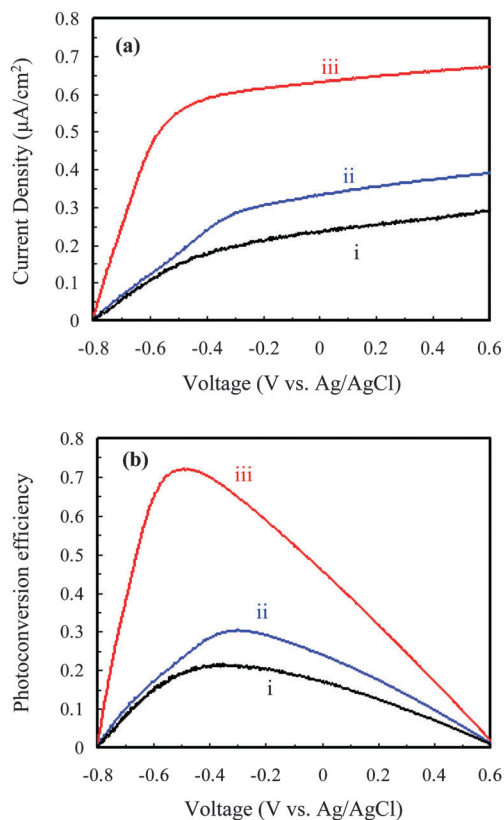This journal is © the Owner Societies 2014

Fig. 7 (a) Linear sweep voltammograms and (b) photoconversion efficiency measured from different photoanodes: (i) P25, (ii) TiO$_2$ single crystals and (iii) TiO$_2$ mesocrystals under light illumination.

potential can be converted from the Ag/AgCl reference electrode *via* the Nernst equation:[39]

$$E_{RHE} = E_{Ag/AgCl} + 0.059 \text{ pH} + E^0_{Ag/AgCl}$$

where $E_{Ag/AgCl}$ is the experimental potential against the Ag/AgCl reference electrode, and $E^0_{Ag/AgCl}$ is the standard potential of Ag/AgCl (0.2 V). The results were shown in Fig. 7b, the TiO$_2$ mesocrystals achieved the highest efficiency of $\sim 0.72\%$ at a low bias of -0.50 V *versus* Ag/AgCl, while the TiO$_2$ single crystals achieved $\sim 0.3\%$ at -0.29 V and P25 achieved $\sim 0.3\%$ at -0.31 V *versus* Ag/AgCl. Thus, our results reveal that the TiO$_2$ mesocrystals possess a significantly increased photocurrent, leading to much improved photoconversion efficiency.

To shed light on why the anatase TiO$_2$ mesocrystals show much enhanced performance in PEC cells, the intrinsic properties of the different photoanode materials were further investigated. UV-vis absorption spectra of different samples are shown in Fig. 8. For all the samples, a significant increase in the absorption at wavelengths shorter than 400 nm can be assigned to the intrinsic bandgap absorption of anatase TiO$_2$ (~ 3.2 eV). P25 shows the best absorption of ultraviolet light, this may be due to the smallest size (~ 20 nm). Therefore, the absorption of ultraviolet light could not be the cause of improved PEC performance of TiO$_2$ single crystals and mesocrystals under these measurement conditions. BET surface area of P25 is 44 m^2 g^{-1}, which is larger than TiO$_2$ single crystals (32 m^2 g^{-1}), but smaller than TiO$_2$ mesocrystals (88 m^2 g^{-1}). Thus, the surface area was not the reason for the increased photocurrent of TiO$_2$ single crystals, but may be a favorable factor for TiO$_2$ mesocrystals with highest photoconversion efficiency.

Electrochemical impedance spectroscopy (EIS) was used to investigate the photogenerated charge separation process of the different photoanodes, and the results are shown in Fig. 9. The radius of the arc on the EIS Nyquist plot reflects the reaction rate occurring at the surface of the electrode. The arc radius on the EIS Nyquist plot of TiO$_2$ mesocrystals is smallest compared with TiO$_2$ single crystals and P25, indicating a most effective separation of photogenerated electron–hole pairs and a fastest interfacial charge transfer.[20,40] This could be attributed to the mesoscopic structure of TiO$_2$ mesocrystals composed of
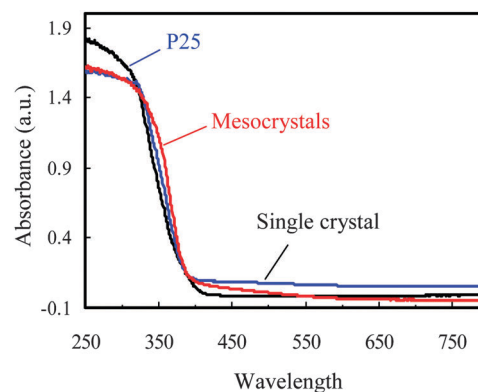
transport distance and highly oriented nanocrystal subunits, and thus would promise better photochemical properties. Fig. 7a shows the typical current–voltage characteristics measured from different photoanodes in a potential window between -0.8 and 0.6 V *versus* Ag/AgCl. When the light was irradiated on the samples, the photocurrent density of all the photoanodes increased with the increasing applied potential. The photocurrent density of the commercial P25 (Degussa) was 0.14 and 0.23 mA cm^{-2} at -0.5 and 0 V *versus* Ag/AgCl, respectively. Compared with TiO$_2$ single crystals and mesocrystals, the photocurrent density of 0.17 (-0.5 V) and 0.33 mA cm^{-2} (0 V) for the former and 0.55 (-0.5 V) and 0.63 mA cm^{-2} (-0.5 V) for the latter was obtained, respectively. Therefore, the TiO$_2$ mesocrystals exhibit much enhanced photocurrent, almost 191% and 274% compared with that of TiO$_2$ single crystals and commercial P25 at the applied potential of 0 V *versus* Ag/AgCl, respectively. In order to quantitatively evaluate the efficiency of PEC hydrogen generation from different photoanodes, the photoconversion efficiency is calculated based on the equation:[2]

$$\eta = I_{mc} \left(1.23 \text{ V} - V_{app}\right)/J_{in}$$

where V_{app} is the applied voltage *versus* reversible hydrogen electrode (RHE), I_{mc} is the external current density at the measured potential, and J_{in} is the power density of the illumination (86 mW cm^{-2}). The reversible hydrogen electrode (RHE)

Fig. 8 UV-visible absorbance spectra of P25, TiO$_2$ single crystals and TiO$_2$ mesocrystals.

This journal is © the Owner Societies 2014

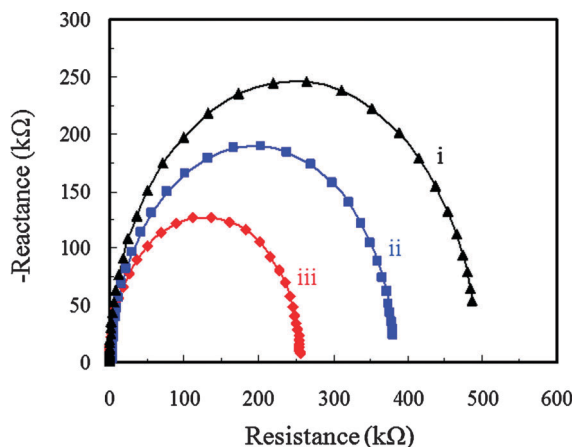*Phys. Chem. Chem. Phys.*, 2014, **16**, 7441–7447 | 7445

Fig. 9 EIS Nyquist plots of (i) P25, (ii) TiO$_2$ single crystals and (iii) TiO$_2$ mesocrystals under light illumination.

highly ordered nanocrystal subunits, which offer large surface area, nanoporous nature and a short transport distance, and thus facilitate the well contact between the electrode and the electrolyte, the effective charge separation of electron–hole pairs and fast interfacial charge transfer. On the other hand, the TiO$_2$ single crystals exhibit a smaller interfacial charge transfer resistance than that of P25, this may be because the relatively large single crystals have a higher electron mobility than that of small nanoparticles,[12] and/or the {101} facets of anatase are more photoactive for hydrogen production.[41] Hence, it could be concluded that the effective charge separation of electron–hole pairs and fast interfacial charge transfer are significantly critical for the efficient PEC conversion. Actually, some intrinsic limitations of photoelectrodes such as short hole diffusion lengths or low electron mobility could be overcame by tailoring of both the size of the nanoparticles and the film porosity, but this strategy will bring on enhanced charge recombination due to the increased surface area in contact with the electrolyte or the electron trapping/scattering at grain boundaries.[13,42] Herein, the mesocrystals with "single-crystal-like" structure, offering the advantages of both nanoporous nature and few grain boundaries arising from crystallographically oriented nanocrystal subunits, could be ideal material for simultaneously addressing these problems. It may be reasonably expected that the PEC performance of the mesocrystals could be further improved through the optimization of the mesocrystalline architectures.

Conclusions

Anatase TiO$_2$ mesocrystals and single crystals with dominant {101} facets were successfully synthesized without additives using titanate nanowires as precursors under solvothermal and hydrothermal conditions, respectively. It is proposed that the anatase mesocrystals were formed through the oriented self-assembly process of anatase nanocrystal subunits, and the anatase single crystals were formed through the dissolution and recrystallization of TiO$_2$–B nanorods. Nevertheless, the growth of anatase TiO$_2$ mesocrystals was controlled by the

same thermodynamic principle as that of single crystals in this simple reaction system. Furthermore, the TiO$_2$ mesocrystals were used as PEC anodes and demonstrated much enhanced photocurrent, almost 191% and 274% compared with that of TiO$_2$ single crystals and commercial P25, respectively. The EIS measurements under illumination proved that the photocurrent increase was largely ascribed to the effective charge separation of electron–hole pairs and fast interfacial charge transfer, arising from the intrinsic characteristics of the mesostructured TiO$_2$ composed of highly ordered nanocrystal subunits offering few grain boundaries, nanoporous nature and a short transport distance. These results may provide a new insight to controllably fabricate mesocrystals of other semiconductor nanomaterials, and thus promote their applications in photochemical devices.

Acknowledgements

Notes and references

1 A. I. Hochbaum and P. Yang, *Chem. Rev.*, 2009, **110**, 527–546.
2 M. G. Walter, E. L. Warren, J. R. McKone, S. W. Boettcher, Q. Mi, E. A. Santori and N. S. Lewis, *Chem. Rev.*, 2010, **110**, 6446–6473.
3 A. B. Murphy, P. R. F. Barnes, L. K. Randeniya, I. C. Plumb, I. E. Grey, M. D. Horne and J. A. Glasscock, *Int. J. Hydrogen Energy*, 2006, **31**, 1999–2017.
4 Y. Wang, T. Wang, P. Da, M. Xu, H. Wu and G. Zheng, *Adv. Mater.*, 2013, **25**, 5177–5195.
5 A. Fujishima and K. Honda, *Nature*, 1972, **238**, 37–38.
6 A. L. Linsebigler, G. Lu and J. T. Yates, *Chem. Rev.*, 1995, **95**, 735–758.
7 X. Chen and S. S. Mao, *Chem. Rev.*, 2007, **107**, 2891–2959.
8 M. Ni, M. K. H. Leung, D. Y. C. Leung and K. Sumathy, *Renewable Sustainable Energy Rev.*, 2007, **11**, 401–425.
9 K. Sivula, F. Le Formal and M. Grätzel, *ChemSusChem*, 2011, **4**, 432–449.
10 R. Franking, L. Li, M. A. Lukowski, F. Meng, Y. Tan, R. J. Hamers and S. Jin, *Energy Environ. Sci.*, 2013, **6**, 500–512.
11 Y. Qiu, K. Yan, H. Deng and S. Yang, *Nano Lett.*, 2011, **12**, 407–413.
12 E. Hendry, M. Koeberg, B. O'Regan and M. Bonn, *Nano Lett.*, 2006, **6**, 755–759.
13 K. Sivula, F. Le Formal and M. Grätzel, *ChemSusChem*, 2011, **4**, 432–449.
14 P. Roy, S. Berger and P. Schmuki, *Angew. Chem., Int. Ed.*, 2011, **50**, 2904–2939.
15 G. Wang, H. Wang, Y. Ling, Y. Tang, X. Yang, R. C. Fitzmorris, C. Wang, J. Z. Zhang and Y. Li, *Nano Lett.*, 2011, **11**, 3026–3033.
16 I. S. Cho, M. Logar, C. H. Lee, L. Cai, F. B. Prinz and X. Zheng, *Nano Lett.*, 2013, **14**, 24–31.

7446 | *Phys. Chem. Chem. Phys.*, 2014, **16**, 7441–7447

This journal is © the Owner Societies 2014

17 I. S. Cho, Z. Chen, A. J. Forman, D. R. Kim, P. M. Rao, T. F. Jaramillo and X. Zheng, *Nano Lett.*, 2011, **11**, 4978–4984.

18 J. Shi, Y. Hara, C. Sun, M. A. Anderson and X. Wang, *Nano Lett.*, 2011, **11**, 3413–3419.

19 D. Feng, W. Luo, J. Zhang, M. Xu, R. Zhang, H. Wu, Y. Lv, A. M. Asiri, S. B. Khan, M. M. Rahman, G. Zheng and D. Zhao, *J. Mater. Chem. A*, 2013, **1**, 1591–1599.

20 Z. Jiang, Y. Tang, Q. Tay, Y. Zhang, O. I. Malyi, D. Wang, J. Deng, Y. Lai, H. Zhou, X. Chen, Z. Dong and Z. Chen, *Adv. Energy Mater.*, 2013, **3**, 1368–1380.

21 H. Cölfen and M. Antonietti, *Angew. Chem., Int. Ed.*, 2005, **44**, 5576–5591.

22 D. V. Talapin, J.-S. Lee, M. V. Kovalenko and E. V. Shevchenko, *Chem. Rev.*, 2010, **110**, 389–458.

23 H. Goesmann and C. Feldmann, *Angew. Chem., Int. Ed.*, 2010, **49**, 1362–1395.

24 R. Q. Song and H. Cölfen, *Adv. Mater.*, 2010, **22**, 1301–1330.

25 L. Zhou and P. O'Brien, *Small*, 2008, **4**, 1566–1574.

26 J. Ye, W. Liu, J. Cai, S. Chen, X. Zhao, H. Zhou and L. Qi, *J. Am. Chem. Soc.*, 2011, **133**, 933–940.

27 Z. Hong, M. Wei, T. Lan, L. Jiang and G. Cao, *Energy Environ. Sci.*, 2012, **5**, 5408–5413.

28 Z. Hong, M. Wei, T. Lan and G. Cao, *Nano Energy*, 2012, **1**, 466–471.

29 P. Tartaj and J. M. Amarilla, *Adv. Mater.*, 2011, **23**, 4904–4907.

30 P. Tartaj, *Chem. Commun.*, 2011, **47**, 256–258.

31 S. H. Yu, H. Cölfen, K. Tauer and M. Antonietti, *Nat. Mater.*, 2005, **4**, 51–55.

32 A. N. Kulak, P. Iddon, Y. Li, S. P. Armes, H. Cölfen, O. Paris, R. M. Wilson and F. C. Meldrum, *J. Am. Chem. Soc.*, 2007, **129**, 3729–3736.

33 M. Huang, U. Schilde, M. Kumke, M. Antonietti and H. Cölfen, *J. Am. Chem. Soc.*, 2010, **132**, 3700–3707.

34 M. Niederberger and H. Colfen, *Phys. Chem. Chem. Phys.*, 2006, **8**, 3271–3287.

35 Y. Wang, Z. Hong, M. Wei and Y. Xia, *Adv. Funct. Mater.*, 2012, **22**, 5185–5193.

36 Z. Zhang, X. Zhong, S. Liu, D. Li and M. Han, *Angew. Chem., Int. Ed.*, 2005, **44**, 3466–3470.

37 D. Jiang, Y. Xu, B. Hou, D. Wu and Y. Sun, *Eur. J. Inorg. Chem.*, 2008, 1236–1240.

38 A. S. Barnard and P. Zapol, *Phys. Rev. B: Condens. Matter Mater. Phys.*, 2004, **70**, 235403.

39 S. Hoang, S. Guo, N. T. Hahn, A. J. Bard and C. B. Mullins, *Nano Lett.*, 2012, **12**, 26–32.

40 W. H. Leng, Z. Zhang, J. Q. Zhang and C. N. Cao, *J. Phys. Chem. B*, 2005, **109**, 15008–15023.

41 T. R. Gordon, M. Cargnello, T. Paik, F. Mangolini, R. T. Weber, P. Fornasiero and C. B. Murray, *J. Am. Chem. Soc.*, 2012, **134**, 6751–6761.

42 D. Koziej, A. Lauria and M. Niederberger, *Adv. Mater.*, 2013, **26**, 235–257.